Korean J. Chem. Eng., 37(7), 1166-1173 (2020)
DOI: 10.1007/s11814-020-0546-x

pISSN: 0256-1115
eISSN: 1975-7220

Rapid removal of low concentrations of mercury from wastewater using coal gasification slag

Liangyan Duan*, Xiude Hu, Deshuai Sun*,†, Yongzhuo Liu***, Qingjie Guo**,†, Tongkai Zhang*, and Botao Zhang***

*College of Chemistry & Chemical Engineering, Qingdao University, Qingdao 266071, China
**State Key Laboratory of High-efficiency Utilization of Coal & Green Chemical Engineering, Ningxia University, Yinchuan 750021, China
***Key Laboratory of Clean Chemical Processing of Shandong Province, College of Chemical Engineering, Qingdao University of Science & Technology, Qingdao 266042, China
(*Received 20 November 2019 • Revised 17 March 2020 • Accepted 18 March 2020*)

Abstract−Coal gasification slag (CGS) is a carbon-containing solid waste used as an adsorbent to remove low concentrations of mercury from wastewater in a series of batch tests to assess its adsorption properties and safe storage. The results showed that the adsorption of mercury on CGS was a very rapid and efficient process, and adsorption equilibrium was reached in only 10-40 min. A pseudo-second-order kinetics model provided a better fit to the equilibrium data. The adsorption capacity on CGS was just slightly below the value of active carbon. CGS showed the highest mercury removal efficiency at a solution pH of 4. Although the presence of other metal cations and anions affected the adsorption, CGS showed good selectivity for mercury ions. The adsorption of mercury was not affected by low concentrations of Cr^{3+} or Cu^{2+}. The negative interference of anions on the removal efficiency followed the order: $Cl^{-}>H_2PO_4^{-}>CO_3^{2-}$. The adsorption mechanism related to the functional groups included ion exchange, precipitation, coordination complexation, and surface complexation. Mercury adsorbed on CGS leached very slowly in weakly acidic or basic solution. All results of the study indicate that CGS is an economical and safe adsorbent for potential industrial applications.

Keywords: Coal Gasification Slag, Rapid Adsorption, Mercury, Low Concentration, Leaching

INTRODUCTION

Heavy metal pollution has been a focus for many years, as heavy metal ions are highly toxic, non-metabolizable, and non-biodegradable [1]. Once they enter the food chain, heavy metals accumulate in living organisms and cause many well-known adverse health effects, such as potent neurotoxicity, blood vessel congestion, and kidney damage [1,2]. Of the various heavy metals, mercury including methylmercury and inorganic mercury, is one of the most hazardous environmental pollutants [3]. Methylmercury is easily adsorbed and bioaccumulates in organisms [4] while inorganic mercury easily transforms into methylmercury in aquatic ecosystems. Both natural processes and anthropogenic activities contribute to mercury pollution in ecosystems. The major contributors from anthropogenic activities include fuel combustion, mining, the chlor-alkali industrial process, the plastics industry, and the electronics industry [5].

To reduce the concentration of mercury in wastewater, several alternative methods have been reported in the literature. Conventional methods include chemical precipitation [6], ion exchange [7], coagulation [8], and adsorption [9-12], but most of these processes are time consuming, require high energy inputs and large amounts of chemicals. Moreover, their removal efficiency is not high enough, especially for the wastewater containing low mercury concentrations. Among these techniques, adsorption processes are the most promising for the removal of heavy metal ions from wastewater due to the ability to recycle the adsorbent [13,14], simple design of process [15], effective control of secondary pollution, good selectivity of various mental ions [16,17] and high removal efficiency of low concentrations of mercury [13].

Coal gasification slag (CGS) is solid waste produced from coal gasification in modern coal industries. In China, around 700 coal gasification furnaces are used, and more than 250 million tons of coal was consumed in 2015 [18]. Therefore, reducing the amount of CGS produced is a major challenge to ensure the sustainable development. CGS from entrained-flow coal gasification can be classified as either coarse slag (discharged from the lock hopper), and fine slag (discharged by air flow). Coarse slag, which is a dense and abrasive solid with a low carbon content of about 20%, is used for polishing media, cement kiln feed, landscaping and road surface coating. Fine slag is a porous material with a higher unburned carbon content of around 40%, which is used as an adsorbent or a precursor for activated carbon [19]. CGS from coal water slurry gasification contains 20-40% residual carbon. The characterization and properties of unburned carbon in CGS have been explored by some researches [19,20], and the amount of carbon depends on operational parameters and the coal feed quality. Due to the coexistence of silica and metal oxide in CGS, several studies reported

†To whom correspondence should be addressed.
E-mail: luckysds@163.com, qingjie_guo@163.com
Copyright by The Korean Institute of Chemical Engineers.

the preparation of mesoporous materials by as raw materials [21, 22]. However, the processes were costly and complicated, making it difficult to achieve large-scale industrial production [22].

Obviously, as low cost materials, the applications of CGS were not of concern to researchers. Because of the low BET specific surface areas, there were no advantages in the adsorption of organic compounds. However, CGS can be directly used to remove metal ions due to the abundant structural porosity [20] and the high residual carbon. The aim of this study was to explore the direct application of CGS as a low cost adsorbent for the rapid removal of mercury ions from aqueous solution. When the concentration of mercury ions is low in aqueous, the special porosity in adsorbent favors the rapid process. This work provides a new way of CGS, which will greatly benefit the environment.

EXPERIMENTAL SECTION

1. Adsorbents

Raw CGS included dry pulverized gasification coarse slag (DPGCS) and dry pulverized gasification fine slag (DPGFS) from entrained-flow coal gasification technology, as well as coal-water slurry gasification slag (CWSGS) from coal water slurry gasification. CGS with 40-65 wt% water content was dried and separated by manually shaking stainless steel mesh screens with openings of standard numbers of 200. Particles smaller than 96 μm were collected as adsorbents. Particles were oven-dried at 105 °C for 2 hours to eliminate trace moisture before experiments.

2. Characterization

Fourier-transform infrared spectroscopy (FT-IR) spectra were recorded on a Thermo Nexus 470 Fourier-transform infrared spectrometer (Nicolet) using KBr pellets. The surface morphology and elemental composition of adsorbent samples were characterized by a MIRA3 field emission scanning electron microscope equipped with an energy dispersive X-ray spectrometer (TESCAN). The textural properties of pores were analyzed by nitrogen adsorption-desorption isotherms at liquid nitrogen temperature (−196 °C) using an Autosorb-iQ-MP surface area and porosity analyzer (Quantachrome). Powder X-ray diffraction (XRD) data was collected on a D8 ADVANCE XRD with Cu-Kα radiation (Bruker). X-ray fluorescence (XRF) data was obtained using an XRF1800 fluorescence spectrometer (Shimadzu). Elemental analysis was conducted using a Vario EL cube elemental analyzer (Elementar).

3. Batch Adsorption

Mercury adsorption experiments were carried out using the batch equilibration method. Mercury solutions were prepared by using 5% nitric acid to dilute standard mercury solutions, which were purchased from Beijing TanMo Quality Testing center. The mercury ion concentration was controlled in a range of 5-65 mg·L^{-1}. For batch adsorption experiments, 0.22 g adsorbent was added into 20 mL of mercury solution at pH 4.0±0.1. The mixtures were equilibrated for 100-200 min on a rotary shaker at a constant room temperature (25 °C) and then separated by centrifugation for 10 min at 4,000 rpm. The residual mercury concentrations were determined using an F732-VJ cold atomic adsorption mercury analyzer. All data was reported as the average of three runs conducted on the same day. The adsorption capacity (Q) of mercury on adsorbents was calculated by Eq. (1):

$$Q = (C_0 - C) \times \frac{V}{m} \quad (1)$$

where C_0 and C are the concentrations of Hg^{2+} (mg·L^{-1}) before and after adsorption, respectively, V is the volume of Hg^{2+} solution (L), and m is the mass of adsorbent (g).

4. Leaching Process

To assess the stability of mercury ion on adsorbents, desorption experiments were carried out at room temperature (25 °C). 0.22 g recycled adsorbent (Q=1.9-2.27 mg·g^{-1}) was added into 20 mL solution containing Na^+, Ca^{2+}, HCO_3^- and Cl^-. The mixtures were equilibrated for 24 h on a rotary shaker at room temperature and then separated by centrifugation for 10 min at 4,000 rpm. The concentration of Hg^{2+} in the leaching solution was determined and used to calculate the leaching ratio.

RESULTS AND DISCUSSION

1. CGS Characteristics

The main mineral present in CGS was SiO_2 with small amounts of calcium-, aluminum- and iron-containing compounds, as shown in Table S1. According to the elemental analysis, carbon was abundant in CGS, likely due to residual carbon which resulted in a higher loss on ignition. Due to the abundant functional groups on the surface of CGS, residual carbon helped during the adsorption of Hg^{2+} from wastewater. Significant amounts of sulfur were also found. Reduced sulfur, which originated from -SH, C-S, or sulfides (Fig. S1) has been reported to favor the adsorption and precipitation of mercury [7,23-25]. The isotherm in Fig. S2 shows that CGS followed a Type IV N_2 adsorption/desorption isotherm with an obvious H3 hysteresis loop, suggesting the CGS contained platelike particles with slit-shaped pores [23]. The BET specific surface areas of CGS particles ranged from 46-57 m^2·g^{-1} (Table S2), which was higher than fly ash [26,27]. The average pore size was less than 2 nm, indicating that CGS is a microporous material. The SEM images in Fig. S3 show that some spherical particles and irregular carbon were dispersed among the sheet-like particles in DPGCS and DPGFS. There were also thin sheets without irregular particles in the CWSGS sample in Fig. S3(c). The functional groups, especially oxygen-containing functional groups, on the surface of residual carbon were involved in Hg^{2+} adsorption. As shown in Fig. S4, the peaks near 2,900 cm^{-1} are the characteristic stretching vibration of -CH_2-, and the C=O stretching vibration is located at 1,620 cm^{-1}. Two bands at 1,380 cm^{-1} and 1,059 cm^{-1} correspond to -OH. These oxygen-containing functional groups have been reported to be due to carboxyl, phenolic hydroxyl, and lactone bases [28]. To determine the amount of oxygen-containing functional groups, the Boehm method was used to analyze CGS and the values of carboxyl groups on residual carbon were found to be 1.12, 0.82, and 1.33 mmol·g^{-1} for DPGFS, DPGCS, and CWSGS, respectively. These data corresponded to the approximate carboxyl content on the surface of activated carbon (AC) [29,30], indicating CGS could potentially be used for adsorption.

2. Rapid Adsorption of Mercury on CGS

Due to the low concentration of Hg^{2+} in wastewater (0.01-10 mg·L^{-1}), adsorption was time consuming, thereby equilibrium adsorp-

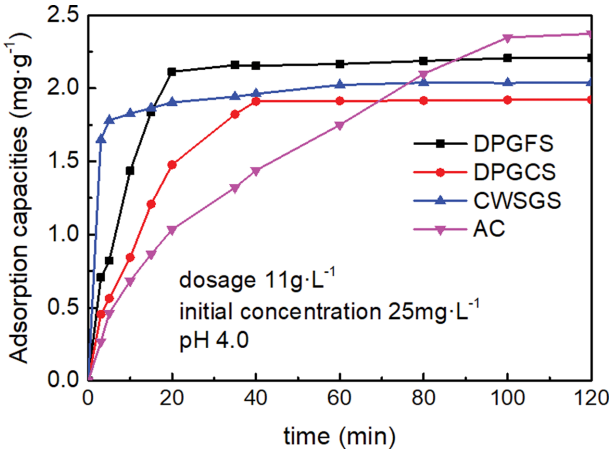


Fig. 1. Effect of time of Hg^{2+} adsorption onto CGS.

tion time is a vital parameter. The effect of time on adsorption was investigated, as shown in Fig. 1. The mercury adsorption on AC, a common commercial adsorbent, was used as a comparison. The adsorption process included a first rapid stage and a second slow stage. The first process was fast because there were many available functional groups on the adsorbent surface, but as these vacant functional groups were occupied, the adsorption kinetics slowed and reached equilibrium. From Fig. 1, the rate of mercury adsorption on AC was rapid in the first 100 min, and then slowly reached equilibrium within 120 min, which was consistent with the results of previous studies [31,32]. In contrast, the adsorption of mercury on CGS was very fast and efficient, with a shorter adsorption time of 20 and 40 min for DPGFS and DPGCS, respectively. Notably, this process finished in only 10 min for CWSGS, possibly due to its special laminated structure and functional groups. Low concentrations of Hg^{2+} were rapidly removed through adsorption, and CGS saved at less 67% treatment time. The adsorption capacity of the three CGS samples ranged from 1.96-2.27 $mg \cdot g^{-1}$, which was slightly lower than the reported value of AC (2.33 $mg \cdot g^{-1}$). Although AC has a higher specific surface area (Table S2), it is a mesopore material, and is not suitable for the removal of Hg^{2+} (ion diameter about 0.24 nm). Therefore, the three CGS samples appeared to be economical adsorbents for potential industrial applications.

The physical and chemical characteristics of adsorbent and adsorbate determine the adsorption kinetics, and the pseudo-first-order kinetics and pseudo-second-order kinetics models are often used to explain surface-controlled adsorption processes [33]. Adsorption involves Fickian diffusion in both the fluid and adsorbent phases, and the effect of diffusion in adsorption processes is described by the Weber-Morris intraparticle diffusion model [34]. All kinetics equations are shown in supporting materials, the linear fits of the kinetics data are presented in Fig. S5, and the calculated parameters are described in Table 1. According to the correlation coefficient (R^2) in Table 1, the pseudo-second-order model better describes the experimental data than the pseudo-first-order kinetics model, indicating that chemical adsorption dominates the adsorption process [27]. According to the pseudo-second-order model, the calculated K_2 values of CGS samples are larger than those of AC, suggesting fast adsorption occurred on CGS. Moreover, the calculated pseudo-second-order equilibrium adsorption capacity is closer to the experimental values, and similar results have been reported by previous studies [24,35]. The rate-controlling mechanism was analyzed by the Weber-Morris intraparticle diffusion model, and the results are presented in Fig. S5 and Table 1. From Fig. S5, the adsorption process is divided into two stages: a rapid external surface adsorption stage and a slow intraparticle diffusion stage [27]. Since the fitting curves of the rapid external surface adsorption stage did not pass through the origin, the rate-controlling step was due to the combined effects surface adsorption and intraparticle diffusion.

Table 2 shows the comparison of adsorption properties between CGS and other low cost adsorbents. All the adsorption processes followed by the pseudo-second-order kinetic model. According to the data, CGS did exhibit rapid removal of mercury from aqueous.

3. Effect of Solution pH on Adsorption

Solution pH greatly affects adsorption because it changes the mercury speciation and also the ionization state of functional groups on the adsorbent surface. The major mercury species was Hg^{2+} at pH<3, and the mixture of Hg^{2+} and $Hg(OH)^{+}$ within a pH range of 3-5 [39]. $Hg(OH)_2$ was the predominant species at pH>5, especially at high mercury concentration [25]. Fig. S6 shows that the points of zero charge (PZC) [26] for DPGFS, DPGCS, and CWSGS were at pH 7.9, 8.1, and 7.1. In acidic solution, all adsorbents are likely positively charged during the experiments, resulting in repul-

Table 1. The parameters of adsorption kinetics

		DPGFS	DPGCS	CWSGS	AC
	Q_{exp} ($mg \cdot g^{-1}$)	2.42	2.84	2.45	3.12
First-order kinetic modal	Q_{cal} ($mg \cdot g^{-1}$)	2.20	1.92	2.04	2.44
	K_1 (min^{-1})	0.0679	0.0927	0.0640	0.0399
	R^2	0.9657	0.9678	0.9805	0.9849
Second-order kinetic modal	Q_{cal} ($mg \cdot g^{-1}$)	2.33	2.14	2.06	2.75
	K_2 ($g \cdot mg^{-1} \cdot min^{-1}$)	0.0883	0.0445	0.4454	0.0264
	R^2	0.9977	0.9934	0.9998	0.9965
Intraparticle diffusion model	K_{31} ($g \cdot mg^{-1} \cdot min^{-1/2}$)	0.4929	0.3422	0.1714	0.0550
	R^2	0.9690	0.9843	0.9018	0.9779
	K_{32} ($g \cdot mg^{-1} \cdot min^{-1/2}$)	0.0167	0.0024	0.0302	0.0027
	R^2	0.9637	0.9730	0.9189	1.0000

Table 2. Comparison of adsorption property by low cost adsorbents according to the second-order kinetic model

Adsorbent	C_0 (mg·L^{-1})	Dosage (g·L^{-1})	Q_{cal} (mg·g^{-1})	K_2 (g·mg^{-1}·min^{-1})	Reference
Biochar from corn straw	0.5	0.33	0.91	6.80e-5 (g·mg^{-1}·h^{-1})	[37]
Biochar from corn straw-NaS	0.5	0.33	1.24	5.49e-5 (g·mg^{-1}·h^{-1})	[37]
Biochar from corn straw-KOH	0.5	0.33	0.98	2.82e-4 (g·mg^{-1}·h^{-1})	[37]
Activated coke	1	0.1	9.64	0.002	[31]
Activated coke-SH	1	0.1	10.00	2.217	[31]
FeS	1	0.12	8.02	7.72e-3	[23]
Pyrite	1	1.0	2.32	1.87e-2	[23]
Calcined *Cardita bicolor* oyster shell	10	5.0	1.968	0.1265	[36]
Activated carbon from waste catalyst	16.55	1.0	14.47	0.017	[35]
DPGFS	25	11.0	2.33	0.0883	This study
DPGCS	25	11.0	2.14	0.0445	This study
CWSGS	25	11.0	2.06	0.4454	This study
Wood biochar	50	2.0	34.2	0.05 (g·mg^{-1}·h^{-1})	[24]
Sulfurized wood biochar	50	2.0	48.1	0.05 (g·mg^{-1}·h^{-1})	[24]
Sugarcane bagasse	76	5.0	14.71	4.46	[38]
Sugarcane bagasse-NaOH	76	5.0	13.89	0.24	[38]
Sugarcane bagasse-HCl	76	5.0	13.88	0.35	[38]

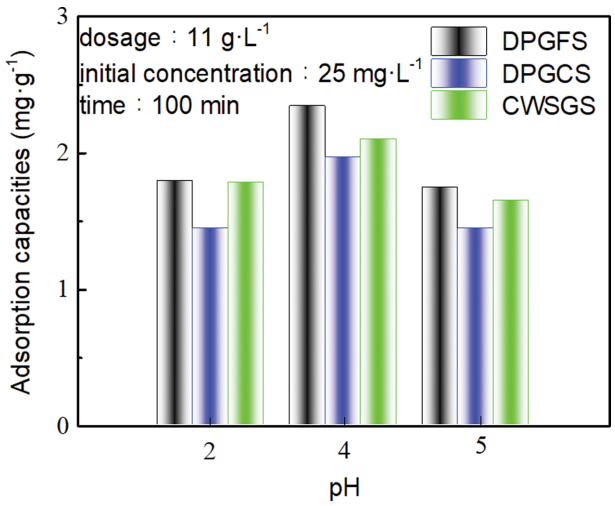


Fig. 2. Effect of solution pH on Hg^{2+} adsorption.

sive electrostatic interactions between adsorbents and mercury ions. Fig. 2 illustrates the effect of solution pH on adsorption and shows that higher removal efficiencies were obtained under acidic solutions, especially at a pH near 4, which is consistent with the previous report [40]. This result indicates that functional groups are vital for the adsorption process and that chemisorption, not physical adsorption, dominates this process. At low pH values, the high concentration of hydronium ion (H_3O^+) possibly competed with Hg^{2+} for active sites on the adsorbent surface, while also preventing the ionization of functional groups. Combined, these hindered the interactions of functional groups with Hg^{2+} and decreased the overall adsorption. At pH 5, the low removal efficient was attributed to the low affinity between surface functional groups and $Hg(OH)^+$. Although about a 25% lower adsorption capacity was observed at different solution pH values, the reduced sulfide in adsorbents was not affected by solution pH [23] and helped maintain higher adsorption capacity of low concentrations of mercury from aqueous solutions.

4. Effect of Coexisting Ions on Adsorption

Generally, wastewater is a multicomponent system that contains multiple metal cations and anions. The metal cations may compete with Hg^{2+} for active sites on the surface of adsorbents, while the anions may form complexes with Hg^{2+}, lowering its affinity for functional groups on the surface of adsorbents. The presence of coexisting ions reduces the removal efficiency, as shown in Fig. 3. From Fig. 3(a), different concentrations of Cr^{3+} or Cu^{2+} were added into simulated wastewater. At low concentrations, Cr^{3+} or Cu^{2+} had little impact on the adsorption of Hg^{2+}, but as their concentrations increased, the removal of Hg^{2+} was reduced. Moreover, Cr^{3+} showed a more competitive adsorption, and led to a 28% reduction in Hg^{2+} removal when it was present in a 40-times molar excess. Although metal cations affected the removal of Hg^{2+}, CGS showed a good selectivity for mercury ions.

The interference of anions was assessed, and the results are shown in Fig. 3(b). Compared with metal cations, anions showed a much greater influence. Cl^- significantly suppressed the uptake of Hg^{2+}, consistent with previous reports [23,31]. The removal efficiency of Hg^{2+} decreased quickly to 54.7% when Cl^- was added, and continuously decreased as the Cl^- concentration further increased. This could be due to the formation of stable $HgCl_x^{2-}$ [23], which had a lower affinity for the adsorbents. $H_2PO_4^-$ also hampered the adsorption process, and resulted in at least a 26.7% reduction in the adsorption capacity of Hg^{2+}. CO_3^{2-}, especially at low concentrations, had little effect on the adsorption process.

5. Leaching of Adsorbed Mercury

To predict whether adsorbed mercury on CGS will be stable in the environment, the leaching of adsorbed mercury was investigated at different solution pH values. Previous reports [41,42] used HCl as a regeneration reagent because increasing the H^+ concentra-

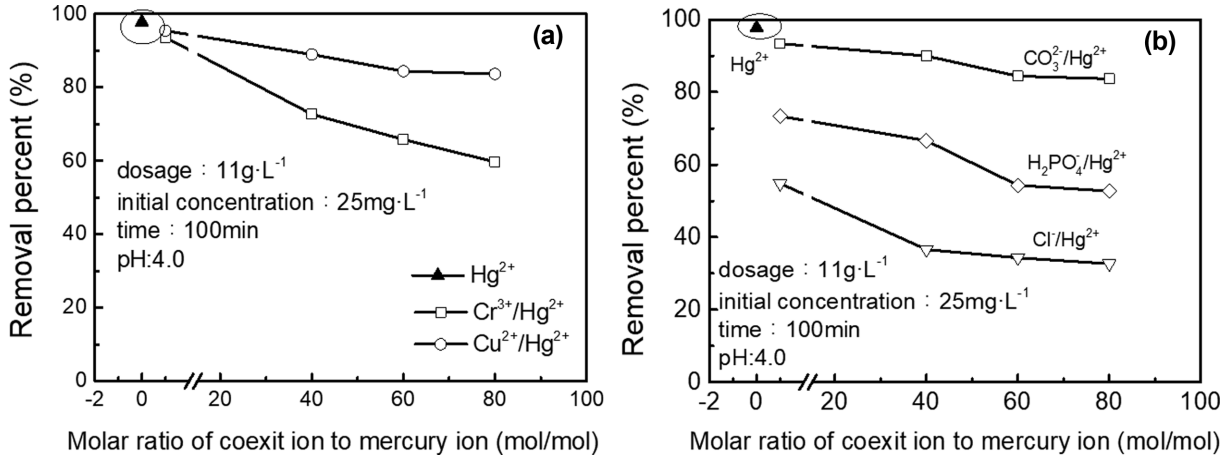


Fig. 3. Effect of coexisting caion (a) and anion (b) on Hg^{2+} adsorption.

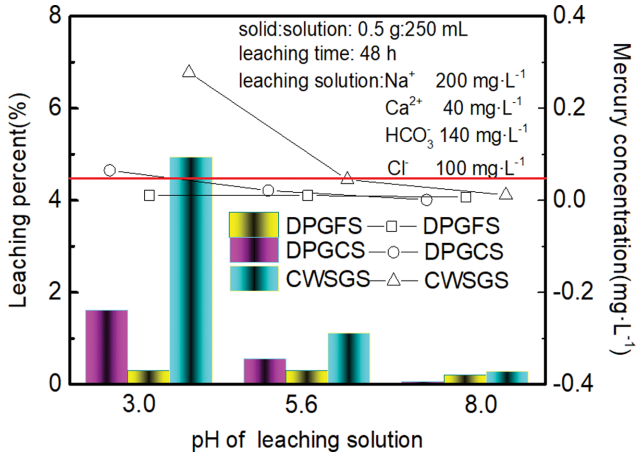


Fig. 4. Effect pH on Hg^{2+} leaching from adsorbed CGS.

tion in the aqueous phase competes with Hg^{2+} ions for binding sites, and the presence of Cl^- may result in the formation of insoluble Hg_2Cl_2. In this leaching experiment, HCl and NaOH were used to adjust the pH of the leaching solution. The results in Fig. 4 illustrate that less than 2% of mercury was leached under weakly acidic and basic conditions, but the leached amount increased as the pH decreased. At pH=5 or 8, the mercury concentration in the leaching solution was less than 0.5 mg·L^{-1}, the discharged standard [43], indicating CGS was stable in natural environment.

6. Adsorption Mechanism

The surface elemental maps of DPGCS, DPGFS, and CWSGS after mercury adsorption were obtained using SEM-EDS and are shown in Fig. S7. More oxygen was observed in spherical particles, which were determined to be metal oxides. The element distributions of C, S and Hg were sporadically dispersed in CGS. Importantly, the amount of Hg^{2+} did not appear to correspond to the presence of a specific element, possibly because the surface elemental content represented the total content which included both inorganic and organic forms, but only organic C/O and reduced S favored the adsorption process. To analyze the mercury content on the surface of CGS, adsorption experiments were carried out in a mercury solution with a concentration of 500 mg·L^{-1}. As shown in Fig. S8, the amount of mercury adsorbed ranged from 0.22-1.2%, which corresponds to 2.2-12 mg·g^{-1}. In fact, the experimental data ranged from 72.5-96.8 mg·g^{-1}. The tremendous differences were due to the enormous amounts of mercury adsorbed into the interior pores of CGS, not just on the surface [44].

To analyze the effect of the surface chemistry of CGS on the adsorption process, samples were also characterized using FT-IR. From Fig. S9, the peaks related to O at 1,650 cm^{-1} and 1,050 cm^{-1}, corresponding to the vibrational peaks of carboxylate and hydroxyl group [45], changed several wavenumbers after adsorption. A new peak at 660 cm^{-1} appeared, which was attributed to O-Hg. These results indicate that the adsorption of Hg^{2+} on CGS involved interactions between carboxylic and hydroxyl groups and Hg^{2+}. The detailed effects of surface elements of CGS on the adsorption process were further characterized using XPS. The XPS survey spectra of CGS before and after mercury adsorption in Fig. S10 contain peaks with binding energies of 104 eV, 164 eV, 285 eV, and 530 eV which correspond to Hg 4f, S2p, C1s, and O1s, respectively. The binding energy of mercury was around 104 eV, which superimposed the silicon peak and significantly increased in intensity after adsorption.

Fig. 5 shows the high-resolution XPS spectra of Hg 4f after mercury adsorption, which shows the presence of three obvious peaks. The peak at 103.8/103.4/103.2 eV corresponds to Si 2p [46], and the two peaks at 100.9 eV and 104.5/104.9/104.0 eV are attributed to Hg4f and represent the spin-orbit splitting of $Hg4f_{5/2}$ and $Hg4f_{7/2}$, respectively [47]. These results indicate that there were multiple adsorption sites in the adsorbents [48]. Adsorbed Hg^{2+} formed inorganic compounds and organic complexes, as indicated by the appearance of two ($Hg4f_{7/2}$ and $Hg4f_{5/2}$) symmetric peaks [31,49].

The XPS O1 s spectra for DPGFS are shown in Fig. 6(a) and (d). A new peak appeared at 533.8 eV after adsorption, which was attributed to O-Hg. The peak at 530.8 eV was assigned to the lattice oxygen (O^{2-}) in inorganic oxides, the content of which did not change after adsorption. This result indicates that O^{2-} did not participate in the adsorption of mercury. Peaks corresponding to C-O and C=O were observed at 532.8 eV and 531.8 eV before mercury adsorption and shifted slightly to 532.9 eV and 532.0 eV after mercury adsorption. Importantly, the C-O content decreased sharply from 50.4% to 39.9%, while the value of C=O decreased slightly from

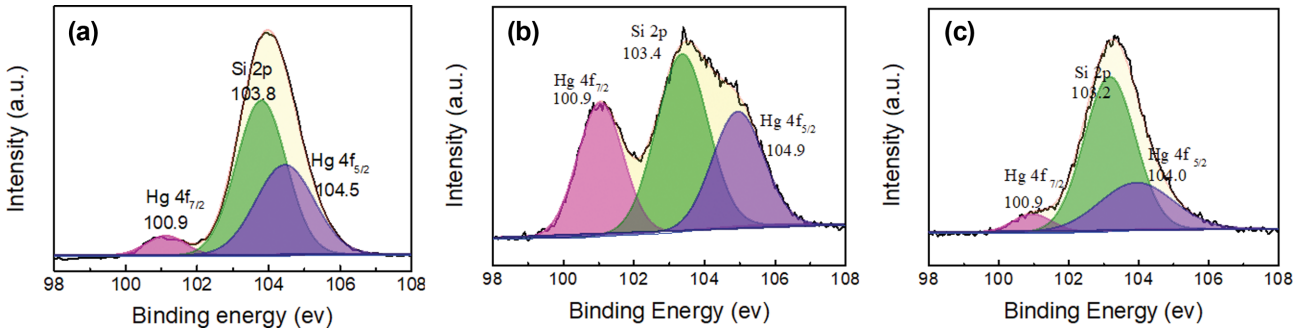


Fig. 5. High-resolution XPS spectra of Hg4f for (a) DPGFS, (b) DPGCS and (c) CWSGS after mercury adsorption.

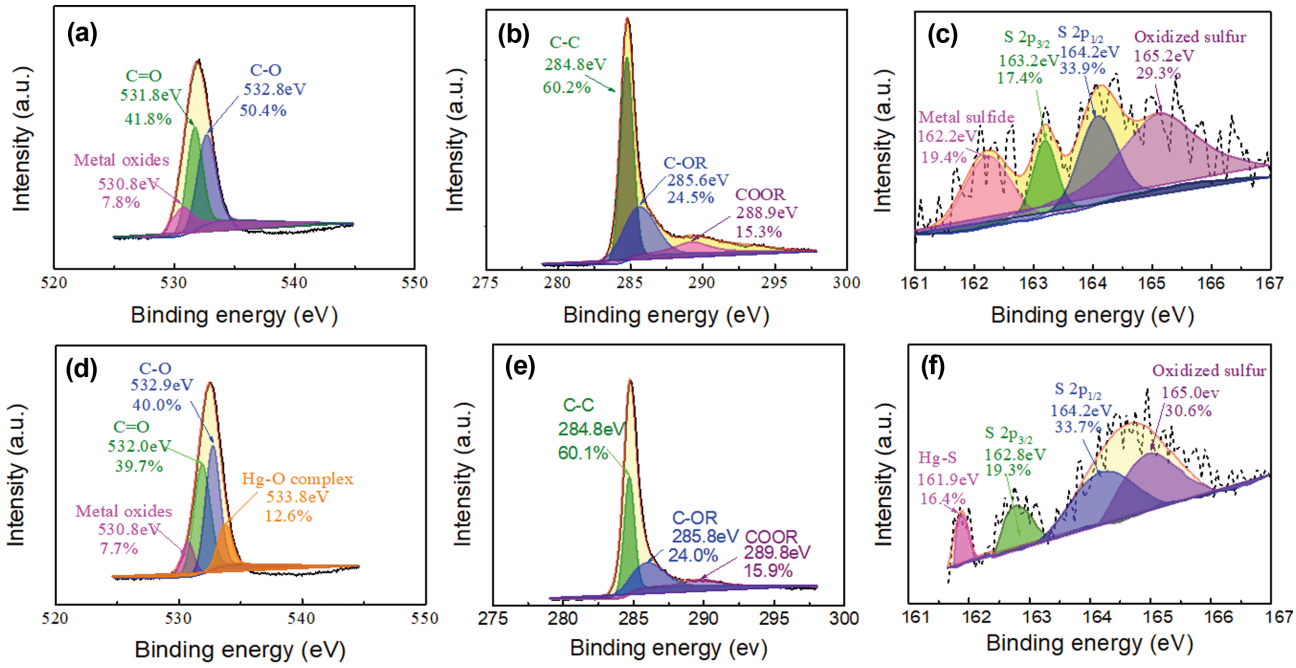


Fig. 6. High-resolution XPS spectra of O (a), C (b) and S (c) before adsorption and O (d), C (e) and S (f) after adsorption for DPGFS.

41.8% to 39.7%. Similar reductions were observed for DPGCS and CWSGS in Fig S11 and Fig S12. Therefore, chemisorbed oxygen C-O was the main functional group which participated in mercury adsorption, and the presence of C=O also promoted adsorption. Most organic oxygen linked with carbon atom. Fig. 6(b) and (e) show that both the binding energy and relative intensities of carbon atoms in DPGFS showed no obvious changes after adsorption, although three carbon-containing functional groups were present C=C (284.8 eV), C-O (285.6/285.8 eV), and C=O (288.9/289.8 eV) [50]. Even for CWSGS, which contained high amounts of residual carbon (Table S1), the main chemical bond in Fig. S12 was C=C, whose content decreased slightly from 81.2% to 80.8%. These results differ from those which showed that C=C was reduced to C-OH during mercury adsorption [29]. However, this may explain why the total adsorption capacity of CWSGS was lower than that of DPGFS because the major residual carbon species had almost no effect on the adsorption process.

The changes of sulfur in DPGFS before and after mercury adsorption are shown in Fig. 6(c) and 6(f). The binding energy at 162.2 eV corresponding to metal sulfide disappeared after adsorption, and a new peak belonging to precipitated HgS appeared at 161.9 eV, indicating that precipitation was the preferential mechanism for sulfur element. The shift in the two peaks at 163.2 eV/164.2 eV to 162.8 eV/164.2 eV after adsorption was assigned to $S2p_{3/2}$ (R-SH) and $S2p_{1/2}$ (C-S), which were reduced sulfur. The sulfur content increased slightly due to mercury adsorption, indicating that reduced sulfur assisted the adsorption process by complexing with Hg-S, in agreement with previous studies [44]. The peaks at 165.2 eV/165.0 eV belonging to oxidized sulfur showed no significant changes before and after adsorption. Similar results were found for DPGCS and CWSGS.

Based on the major Hg^{2+} species, $HgOH^{+}$ and $Hg(OH)_2$, the Hg removal mechanisms under our experimental conditions (pH 4), included ion exchange [35,44] (Eq. (2)-(5)), precipitation (Eq. (6)) [23], coordination complexation [23,44] (Eq 7), and surface complexation [23] (Eq. (8)-(11)).

CONCLUSION

The adsorption of low concentrations of mercury from wastewater using CGS is a fast and efficient process. The adsorption capacity of various CGS samples ranged from 1.96-2.27 $mg \cdot g^{-1}$, which was just slightly below the value of AC (2.33 $mg \cdot g^{-1}$). Adsorption was determined to be a chemical process, and the adsorption data was better described by a pseudo-second-order kinetics model. CGS samples showed higher mercury removal efficiencies in acidic solutions, and the maximum removal was observed in a solution at pH 4. Although metal cations and anions affected

$$RC\text{-}OH/RCO\text{-}OH+Hg^{2+} \rightarrow RC\text{-}O\text{-}Hg\text{-}OCR/RCO\text{-}O\text{-}Hg\text{-}OOCR \quad (2)$$

$$RC\text{-}OH/RCO\text{-}OH+Hg(OH)^{+} \rightarrow RC\text{-}O\text{-}Hg\text{-}OCR/RCO\text{-}O\text{-}Hg\text{-}OOCR \quad (3)$$

$$RC\text{-}OH/RCO\text{-}OH+Hg(OH)_2 \rightarrow RC\text{-}O\text{-}Hg\text{-}OCR/RCO\text{-}O\text{-}Hg\text{-}OOCR \quad (4)$$

$$\text{-}SH+Hg^{2+} \rightarrow \text{-}S\text{-}Hg\text{-} \quad (5)$$

$$S^{2-}+Hg^{2+} \rightarrow HgS \quad (6)$$

$$C\text{-}S+Hg^{2+} \rightarrow C\text{-}S\text{-}Hg \quad (7)$$

$$RC\text{-}OH/RCO\text{-}OH+Hg(OH)^{+} \rightarrow RC\text{-}O\text{-}Hg(OH)^{+}/RCO\text{-}O\text{-}Hg(OH)^{+} \quad (8)$$

$$RC\text{-}OH/RCO\text{-}OH+Hg(OH)_2 \rightarrow RC\text{-}O\text{-}Hg(OH)_2/RCO\text{-}O\text{-}Hg(OH)_2 \quad (9)$$

$$C\text{-}S+Hg(OH)^{+} \rightarrow C\text{-}S\text{-}Hg(OH)^{+} \quad (10)$$

$$C\text{-}S+Hg(OH)_2 \rightarrow C\text{-}S\text{-}Hg(OH)_2 \quad (11)$$

the adsorption of Hg^{2+}, CGS showed a good selectivity for mercury ions. Low molar concentrations of Cr^{3+} or Cu^{2+} had little impact on the adsorption of Hg^{2+}. The interference of anions was intimately associated with ion species, and the removal efficiency of Hg^{2+} decreased quickly to 54.7% upon the addition of Cl^{-}. The presence of $H_2PO_4^{-}$ resulted in at least a 26.7% reduction in the adsorption capacities of Hg^{2+}, but CO_3^{2-} had little effect on the adsorption process. Less than 2% of mercury adsorbed onto CGS was leached at a solution pH of 5 or 8. In a weakly acidic solution, the adsorption mechanisms of mercury on CGS included ion exchange, precipitation, coordination complexation, and surface complexation.

ACKNOWLEDGEMENTS

This work was supported by the Natural Science Foundation of Shandong (ZR2017MB024), Open Project Funding in the Province-Ministry Co-construction Coal Efficient Utilization and Green Chemistry of the State Key Laboratory (2017-K06).

SUPPORTING INFORMATION

Additional information as noted in the text. This information is available via the Internet at http://www.springer.com/chemistry/journal/11814.

REFERENCES

1. N. Huang, L. Zhai, H. Xu and D. Jiang, *J. Am. Chem. Soc.*, **139**, 2428 (2017).
2. B. Davodi, M. Ghorbani and M. Jahangiri, *J. Taiwan Inst. Chem. Eng.*, **80**, 363 (2017).
3. L. Liu, L. Ding, X. Wu and F. Deng, *Ind. Eng. Chem. Res.*, **55**, 51 (2016).
4. P. Wang, R. Wang, C. Wang and J. Qian, *J. Comput. Theor. Nanosci.*, **13**, 5714 (2016).
5. P. Hadi, M. H. To, C. W. Hui, C. S. K. Lin and G. McKay, *Water Res.*, **73**, 37 (2015).
6. M. Cox, EI. EI-Shafey, A. A. Pichugin and Q. Appleton, *J. Chem. Technol. Biotechnol.*, **75**, 427 (2000).
7. Z. Wang, J. Xu, Y. Hu, H. Zhao, J. Zhou, Y. Liu, Z. Lou and X. H. Xiu, *J. Taiwan Inst. Chem. Eng.*, **60**, 394 (2015).
8. J. T. Ackerman, T. E. Kraus, J. A. Fleck, P. K. David, R. H. William, M. B. Sandra, M. P. Herzog, C. A. Hartman and P. A. M. Bachand, *Environ. Sci. Technol.*, **49**, 6304 (2015).
9. X. Yan, J. Meng, X. Hu, R. Feng and M. Zhou, *J. Sol-Gel Sci. Technol.*, **89**, 617 (2019).
10. D. Zhang, Y. Yin and J. Liu, *Chem. Speciat. Bioavailab.*, **29**, 161 (2017).
11. B. Li, Y. Zhang, D. Ma, Z. Shi and S. Ma, *Nat. Commun.*, **5**, 5537 (2014).
12. S. Lone, D. H. Yoon, H. Lee and I. W. Cheong, *Environ. Sci.: Water Res. Technol.*, **5**, 83 (2019).
13. M. Attari, S. S. Bukhari, H. Kazemian and S. Rohani, *J. Environ. Chem. Eng.*, **5**, 391 (2016).
14. Ü. Ecer, Ş. Yılmaz and T. Şahan, *Water Sci. Technol.*, **78**, 1348 (2018).
15. Ş. Yılmaz, A. Zengin, Y. Akbulut and T. Şahan, *Environ. Sci. Pollut. Res.*, **26**, 20454 (2019).
16. Ş. Yılmaz, A. Zengin, Ü. Ecer and T. Şahan, *Colloids Surf. A.*, **583**, 123961 (2019).
17. Y. Uzun and T. Şahan, *Arch. Environ. Prot.*, **43**, 37 (2017).
18. S. Wang, *Chem. Ind. Eng. Prog.*, **35**, 653 (2016).
19. S. Xu, Z. Zhou, X. Gao, G. Yu and X. Gong, *Fuel Process. Technol.*, **90**, 1062 (2009).
20. S. Wu, S. Huang, L. Ji, Y. Wu and J. Gao, *Fuel*, **122**, 67 (2014).
21. Y. Gu and X. Qiao, *Micropor. Mesopor. Mater.*, **276**, 303 (2019).
22. S. Liu, X. Chen, W. Ai and C. Wei, *J. Clean. Prod.*, **212**, 1062 (2019).
23. Y. Sun, D. Lv and J. Zhou, *Chemosphere*, **185**, 452 (2017).
24. J. H. Park, J. Wang, B. Zhou, J. E. R. Mikhael and R. D. DeLaune, *Environ. Pollut.*, **244**, 627 (2019).
25. Ş. Yılmaz, T. Şahan and A. Karabakan, *Korean J. Chem. Eng.*, **34**, 2225 (2017).
26. D. Sun, X. Zhang, Y. Wu and X. Liu, *J. Hazard. Mater.*, **181**, 335 (2010).
27. Y. Wang and D. Sun, *Korean J. Chem. Eng.*, **32**, 1323 (2015).
28. M. Y. Chang and R. S. Juang, *Colloids Surf. A.*, **269**, 35 (2005).
29. E. K. Faulconer and D. W. Mazyck, *J. Environ. Chem. Eng.*, **5**, 2879 (2017).
30. D. Zhang, P. Huo and W. Liu, *Chinese J. Chem. Eng.*, **24**, 446 (2016).
31. Z. Liu, L. Wu, H. Liu, H. Lan and J. Qu, *Chem. Eng. J.*, **228**, 925 (2013).
32. L. Ma, S. M. Islam, C. Xiao, J. Zhao, H. Liu, M. Yuan, G. Sun, H. Li, S. Ma and M. G. Kanatzidis, *J. Am. Chem. Soc.*, **139**, 12745 (2017).
33. A. Azizi, E. Moniri, A. H. Hassani, H. A. Panahi and M. Miralinaghi, *Microchem. J.*, **145**, 559 (2019).
34. Y. Li, H. Xiao, Y. Pan, M. Zhang and Y. Jin, *J. Hazard. Mater.*, **377**, 88 (2019).

35. C. Liu, J. Peng, L. Zhang, S. Wang, S. Ju and C. Liu, *J. Clean. Prod.*, **196**, 109 (2018).
36. A. Teimouri, H. Esmaeili, R. Foroutan and B. Ramavandi, *Korean J. Chem. Eng.*, **35**, 479 (2018).
37. G. Tan, W. Sun, Y. Xu, H. Wang, and N. Xu, *Bioresour. Technol.*, **211**, 727 (2016).
38. A. E. Khoramzadeh, B. Nasemejad and R. Halladj, *J. Taiwan Inst. Chem. E.*, **44**, 266 (2013).
39. N. K. Gupta and A. Gupta, *FlatChem.*, **11**, 1 (2018).
40. K. Aghdam, H. A. Panahi, E. Alaei, A. H. Hasani and E. Moniri, *Environ. Monit. Assess.*, **188**, 223 (2016).
41. A. M. Muliwa, M. S. Onyango, A. Maity and A. Ochieng, *Water Sci. Technol.*, **75**, 2841 (2017).
42. M. K. Alomar, M. A. Alsaadi, T. M. Jassam, S. Akib, M. A. Hashim and C. Schwandt, *J. Colloid Interface Sci.*, **497**, 413 (2017).
43. GB8978-1996, *Integrated wastewater discharge standard*, Publications, Beijing (1996).
44. P. Liu, C. J. Ptacek, D. W. Blowes and R. C. Landis, *J. Hazard. Mater.*, **308**, 233 (2016).
45. P. Hadi, M. H. To, C. W. Hui, C. S. K. Li and G. Mckay, *Water Res.*, **73**, 37 (2015).
46. N. D. Hutson, B. C. Attwood and K. G. Scheckel, *Environ. Sci. Technol.*, **41**, 1747 (2007).
47. A. S. K. Kuma, S. J. Jiang and W. L. Tseng, *J. Environ. Chem. Eng.*, **4**, 2052 (2016).
48. E. Magni and G. A. Somorjai, *Appl. Surf. Sci.*, **89**, 187 (1995).
49. A. S. K. Kumar and S. J. Jiang, *RSC Adv.*, **5**, 6294 (2015).
50. Y. Guan, T. Hu, J. Wu, L. Zhao, F. Tian, W. Pan, P. He, X. Qi, F. Li and K. Xu, *Korean J. Chem. Eng.*, **36**, 115 (2019).

Supporting Information

Rapid removal of low concentrations of mercury from wastewater using coal gasification slag

Liangyan Duan*, Xiude Hu, Deshuai Sun*,†, Yongzhuo Liu***, Qingjie Guo**,†, Tongkai Zhang*, and Botao Zhang***

*College of Chemistry & Chemical Engineering, Qingdao University, Qingdao 266071, China
**State Key Laboratory of High-efficiency Utilization of Coal & Green Chemical Engineering, Ningxia University, Yinchuan 750021, China
***Key Laboratory of Clean Chemical Processing of Shandong Province, College of Chemical Engineering, Qingdao University of Science & Technology, Qingdao 266042, China
(*Received 20 November 2019 • Revised 17 March 2020 • Accepted 18 March 2020*)

Adsorption Kinetics

The physical and chemical characteristics of the adsorbent and adsorbate determined the adsorption kinetics. The pseudo-first-order kinetics and pseudo-second-order kinetics often were used to explain the adsorption process [1-3]. The diffusion effect in adsorption process was revealed by Weber-Morris intraparticle diffusion model

Table S1. Properties of CGS

Samples	Chemical composition (wt%)							Element analysis (wt%)				Loss on ignition (wt%)
	Al_2O_3	CaO	Fe_2O_3	SiO_2	SO_2	K_2O	Others	N	C	H	S	
DPGFS	14.66	14.51	11.47	43.32	4.62	2.29	9.13	0.39	25.33	0.90	1.95	11.92
DPGCS	13.95	14.13	17.55	42.42	3.05	2.17	6.70	0.36	16.63	0.83	1.33	4.33
CWSGS	15.93	19.23	11.44	38.12	5.01	2.28	7.98	1.24	65.41	3.72	2.03	47.67

Table S2. Specific surface area and pore structure parameter of CGS

Samples	Specific surface area ($m^2 \cdot g^{-1}$)	Average pore size (nm)	Mesoporous volume ($cm^3 \cdot g^{-1}$)	Microporous volume ($cm^3 \cdot g^{-1}$)
DPGFS	57.786	0.510	0.099	0.104
DPGCS	50.422	0.810	0.076	0.074
CWSGS	46.775	1.660	0.065	0.056
AC	386.658	4.118	0.318	0.088

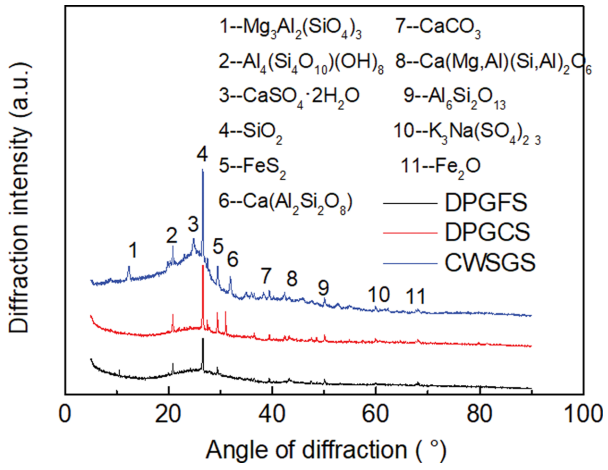


Fig. S1. XRD spectrum of CGS.

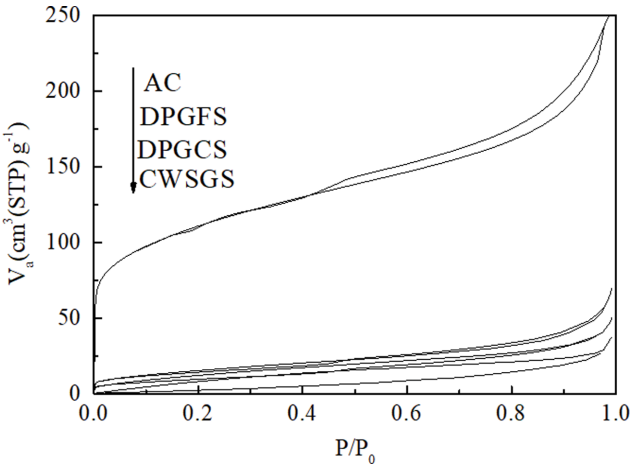


Fig. S2. N_2 adsorption/desorption curve.

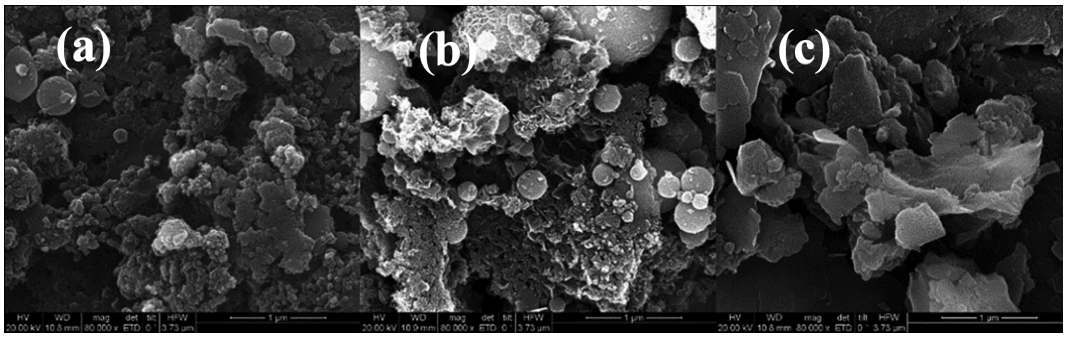


Fig. S3. SEM photos of (a) DPGFS (b) DPGCS and (c) CWSGS.

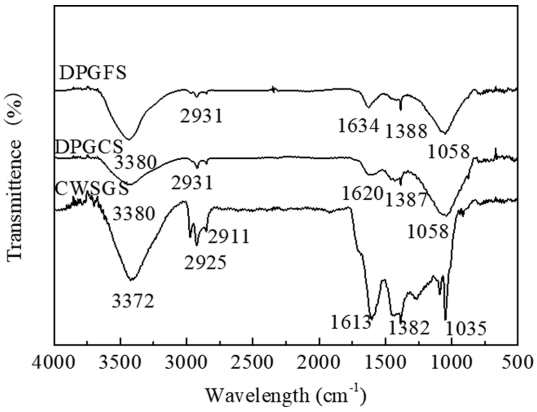


Fig. S4. FTIR of original CGS.

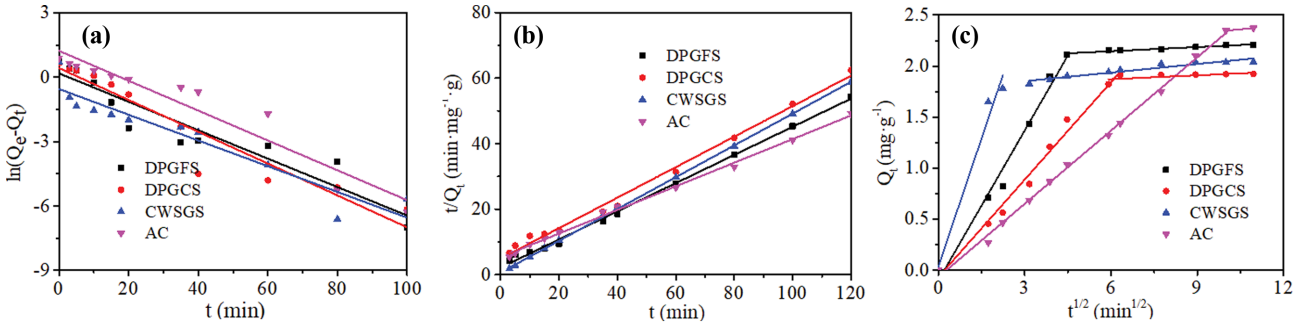


Fig. S5. Linear fitting of pseudo-first-order kinetics (a), pseudo-second-order reaction kinetics (b) and Weber-Morris equation (c).

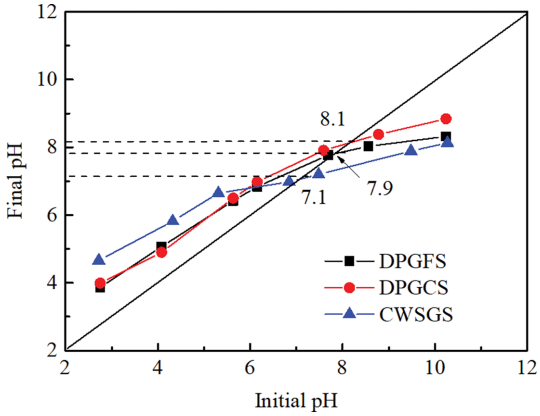


Fig. S6. The points of zero charges of CGS.

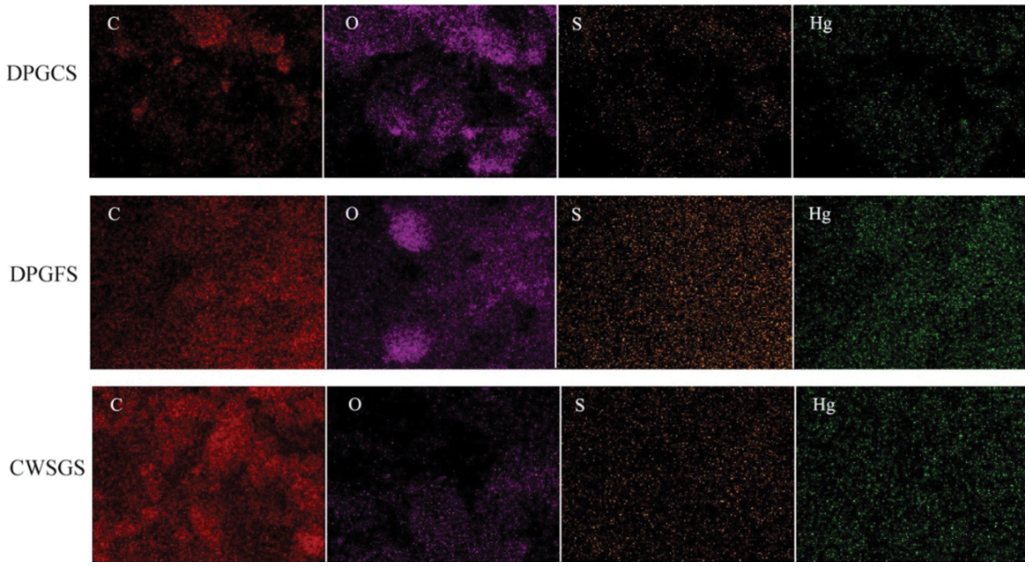


Fig. S7. SEM - Element mapping after mercury adsorption of DPGFS (a), DPGCS (b) and CWSGS (c).

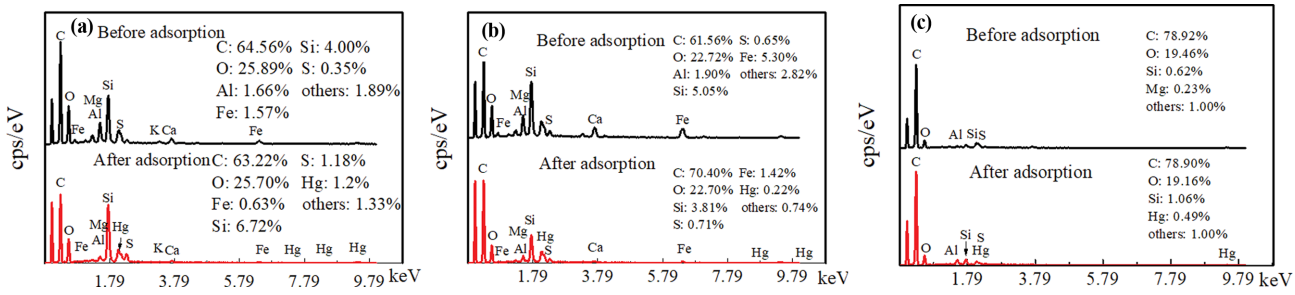


Fig. S8. SEM-EDS spectra of (a) DPGFS, (b) DPGCS and (c) CWSGS before and after adsorption.

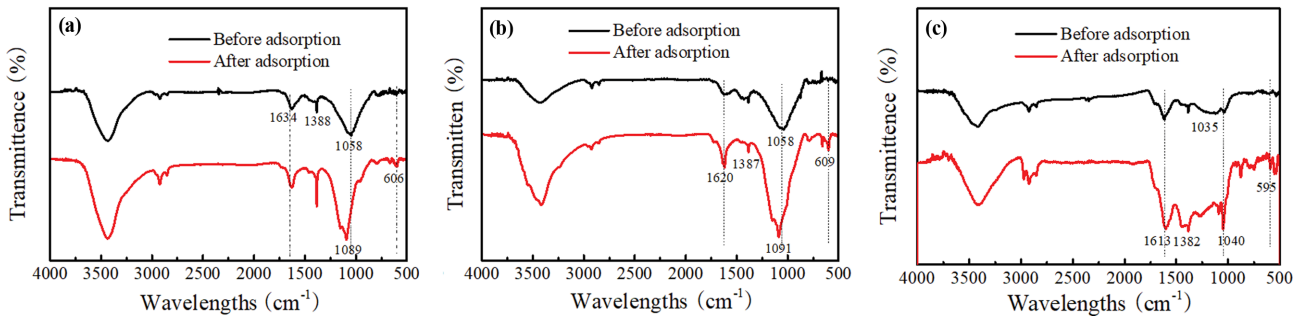


Fig. S9. FT-IR spectra of (a) DPGFS, (b) DPGCS and (c) CWSGS before and after adsorption.

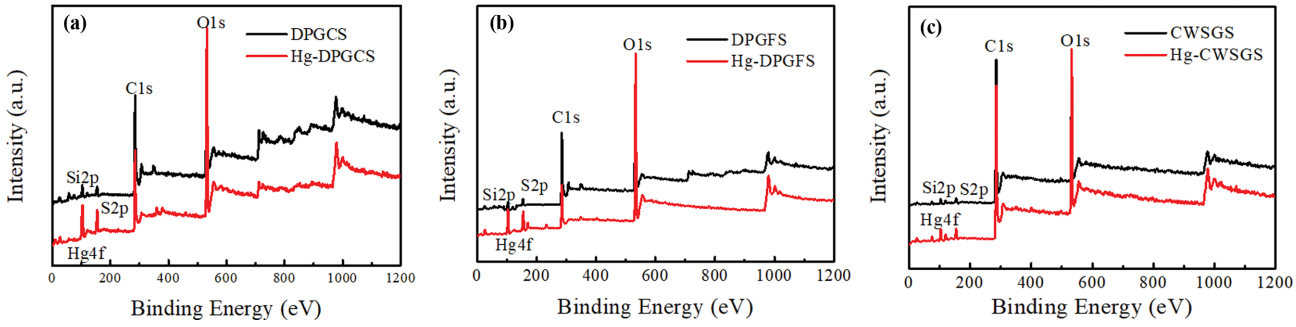


Fig. S10. XPS survey spectra of (a) DPGFS, (b) DPGCS and (c) CWSGS.

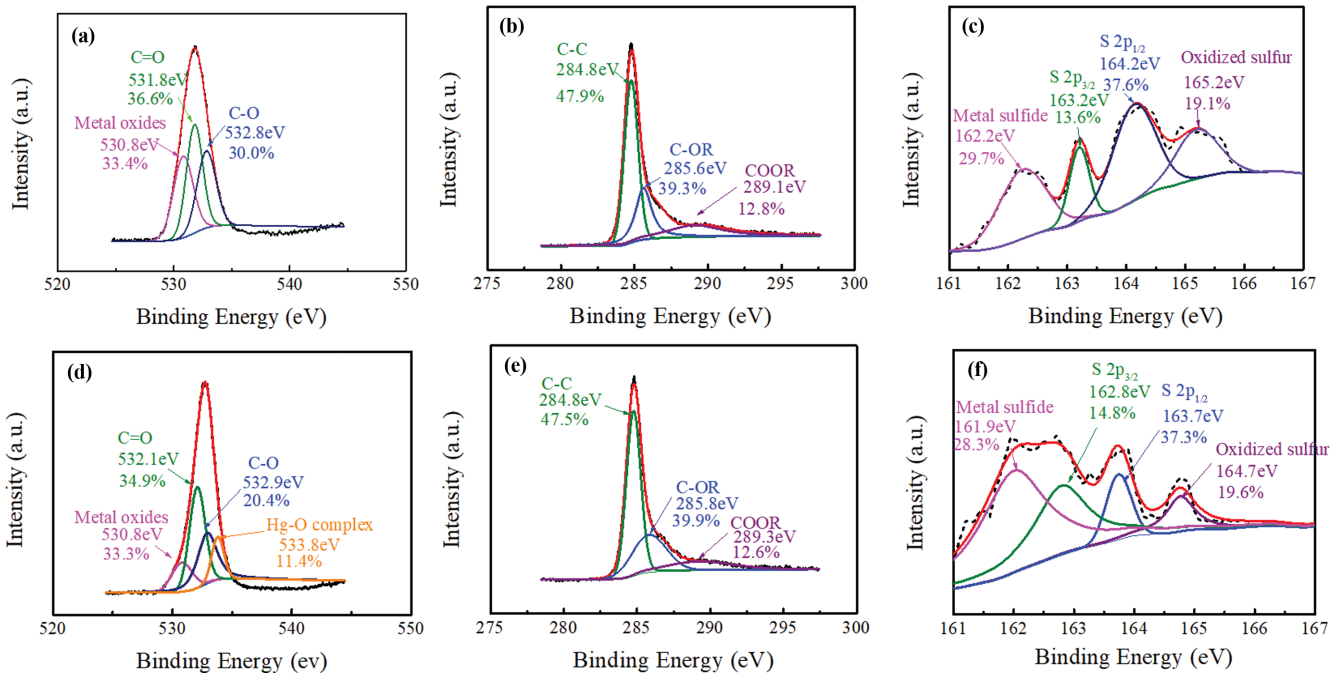


Fig. S11. High-resolution XPS spectra of O (a), C (b) and S (c) before adsorption and O (d), C (e) and S (f) after adsorption for DPGCS.

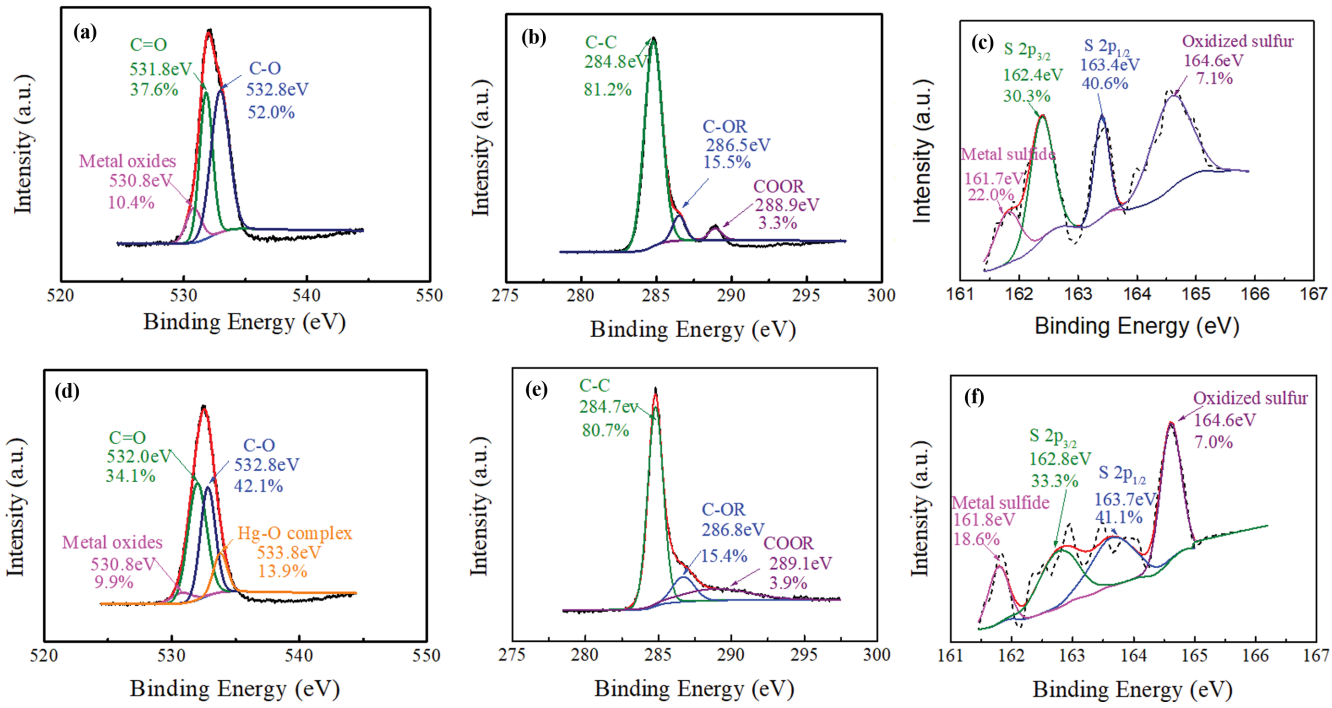


Fig. S12. High-resolution XPS spectra of O (a), C (b) and S (c) before adsorption and O (d), C (e) and S (f) after adsorption for CWSGS.

[4,5]. The linear forms for the models are presented as follows:

$$\ln(Q_e - Q_t) = \ln Q_e - K_1 t \quad (1)$$

$$\frac{t}{Q_t} = \frac{1}{K_2 Q_e^2} + \frac{t}{Q_e} \quad (2)$$

$$Q_t = K_3 t^{1/2} + C \quad (3)$$

Where Q_t and Q_e are the adsorption capacity at time t and at equilibrium ($mg \cdot g^{-1}$), respectively. K_1 represents pseudo-first-order reaction kinetics rate constant (min^{-1}), and K_2 is the pseudo-second-order equilibrium rate constant ($g \cdot mg^{-1} \cdot min^{-1}$). K_{3i} is the rate constant of intraparticle diffusion at the stage i ($mg \cdot g^{-1} \cdot min^{-1/2}$), C_i is the intercept at different stages and t is the adsorption time (min).

REFERENCES

1. A. Azizi, E. Moniri, A. H. Hassani, H. A. Panahi and M. Miralinaghi, *Microchem. J.*, **145**, 559 (2019).
2. M. Y. Chan and R. S. Juang, *Colloids Surf. A*, **269**(1-3), 35 (2015).
3. T. Anitha, P. Senthil Kumar and K. Sathish Kumar, *Environ. Pro. Sustain Energy*, **34**(1), 15 (2015).
4. Y. Li, H. Xiao, Y. Pan, M. Zhang and Y. Jin, *J. Hazard. Mater.*, **377**, 88 (2019).
5. D. Sun, X. Zhang, Y. Wu and T. Liu, *Int. J. Environ. Sci. Technol.*, **10**(4), 799 (2013).